An Anion Binding Site in Human Aldose Reductase: Mechanistic Implications for the Binding of Citrate, Cacodylate, and Glucose 6-Phosphate[†,‡]

David H. Harrison,[§] Kurt M. Bohren,[∥] Dagmar Ringe,[§] Gregory A. Petsko,[§] and Kenneth H. Gabbay*[,§,∥]

Molecular Diabetes and Metabolism Section, Departments of Pediatrics and Cell Biology, Baylor College of Medicine, Houston, Texas 77030, and The Rosenstiel Basic Medical Sciences Research Center, Brandeis University, Waltham, Massachusetts 02554

Received October 11, 1993; Revised Manuscript Received December 13, 1993[⊛]

ABSTRACT: Aldose reductase is a NADPH-dependent aldo–keto reductase involved in the pathogenesis of some diabetic and galactosemic complications. The published crystal structure of human aldose reductase [Wilson et al. (1992) *Science 257*, 81–84] contains a hitherto unexplained electron density positioned within the active site pocket facing the nicotinamide ring of the NADPH and other key active site residues (Tyr48, His110, and Cys298). In this paper we identify the electron density as citrate, which is present in the crystallization buffer (pH 5.0), and provide confirmatory evidence by both kinetic and crystallographic experiments. Citrate is an uncompetitive inhibitor in the forward reaction with respect to aldehyde (reduction of aldehyde), while it is a competitive inhibitor with respect to alcohol in the backward reaction (oxidation of alcohol), indicating that it interacts with the enzyme–$NADP^+$–product complex. Citrate can be replaced in the crystalline enzyme complex by cacodylate or glucose 6-phosphate; the structure of each of these complexes shows the specific molecule bound in the active site. All of the structures have been determined to a nominal resolution of 1.76 Å and refined to *R*-factors below 18%. While cacodylate can be bound within the active site under the crystallization conditions, it does not inhibit the wild-type enzyme in solution. Glucose 6-phosphate, however, is a substrate for aldose reductase. The similar location of the negative charges of citrate, cacodylate, and glucose 6-phosphate within the active site suggests an anion-binding site delineated by the C4N of nicotinamide, the OH of Tyr48, and the Nε of His110. The location of citrate binding in the active site leads to a plausible catalytic mechanism for aldose reductase.

Aldose reductase (EC 1.1.1.21) is a member of the aldo–keto reductase superfamily which catalyzes the NADPH[1]-dependent reduction of a variety of carbonyl compounds (Bachur, 1976; Bohren et al., 1989). Its ability to reduce glucose and galactose to their respective sugar alcohols has been implicated in the pathogenesis of some diabetic and galactosemic complications affecting the lens, retina, nerves, and kidneys (Gabbay, 1973; Kinoshita, 1974; Kador, 1988).

Aldose reductase has been crystallized, and its X-ray crystallographic structure has been determined (Rondeau et al., 1992; Wilson et al., 1992). The human aldose reductase enzyme structure (Wilson et al., 1992), refined at 1.65-Å resolution and an *R*-factor of 20%, contains a hitherto unexplained electron density within the active site pocket. This unidentified electron density sits atop the "A"[2] face or solvent-exposed side of the nicotinamide ring where the substrate or product might be bound. The unidentified electron density is thus surrounded by the putative active site residues, Tyr48, His110, and Cys298 (Wilson et al., 1992).

Herein we report the refined structure of human aldose reductase, crystallized as previously described (Wilson et al., 1992), at a resolution of 1.8 Å and refined to an *R*-factor of 16.9%. The unknown electron density is clearly resolved as citrate, which is present at a 25 mM concentration during crystallization. Citrate replacement studies in aldose reductase crystals with cacodylate and glucose 6-phosphate verify that the active site electron density is indeed citrate. Enzyme kinetics indicate that citrate is an aldose reductase inhibitor and glucose 6-phosphate is a substrate. The combined structure and function studies with these negatively charged compounds indicate the presence of an anion binding site within the active site pocket. Citrate, serendipitously used in the crystallization media, provides a unique crystal form and also allows a credible proposal to be made for the catalytic mechanism of aldose reductase.

METHODS

Crystallization of Aldose Reductase. Human recombinant aldose reductase was overexpressed in *Escherichia coli* and purified as described in detail elsewhere (Bohren et al., 1991). Aldose reductase crystals were obtained at 4 °C as described earlier (Wilson et al., 1992) by the microdiffusion vapor technique, using poly(ethylene glycol) (PEG) 6000 as the precipitant and a protein concentration of 14 mg/mL, pH 5.0 (25 mM citrate buffer, 7 mM β-mercaptoethanol). The

[†] This work was supported by grants from the National Institutes of Health (DK-39044 and GM-26788), the Juvenile Diabetes Foundation, the Lucille P. Markey Charitable Trust, and the Harry B. and Aileen B. Gordon Foundation. Part of this work was done during a sabbatical by K.H.G. as Visiting Scientist in the laboratory of D.R. and G.A.P. (1992–1993).

[‡] The atomic coordinates and structure factors have been deposited in the Brookhaven Protein Data Bank (references: 1ACS = wild-type enzyme–$NADP^+$–citrate; 1ACR = wild-type enzyme–$NADP^+$–cacodylate; 1ACQ = wild-type enzyme–$NADP^+$–glucose 6-phosphate).

* Address correspondence to this author at the Departments of Pediatrics and Cell Biology, Baylor College of Medicine, 1 Baylor Plaza, Houston, TX 77030 [telephone (713)770-3765; FAX (713)770-3766; internet kgabbay@mbcr.bcm.tmc.edu].

[§] Brandeis University.

[∥] Baylor College of Medicine.

[⊛] Abstract published in *Advance ACS Abstracts,* February 15, 1994.

[1] Abbreviations: PEG, poly(ethylene glycol); β-ME, β-mercaptoethanol; NADPH/$NADP^+$, nicotinamide adenine dinucleotide phosphate, reduced and oxidized forms.

[2] The designation of A face has been changed from our previously published paper (Wilson et al., 1992) to agree with the dehydrogenase literature. The A face of the nicotinamide ring corresponds to the *re* face of $NADP^+$.

0006-2960/94/0433-2011$04.50/0 © 1994 American Chemical Society

droplet of protein was suspended over a well containing 20% PEG in 50 mM citrate buffer, pH 5. Crystals usually took about 3 weeks to reach maximum dimensions of up to 1.2 mm × 0.8 mm × 0.6 mm. The crystals are isomorphous with those previously reported (Wilson et al., 1992).

Wild-type crystals were directly transferred from the hanging drop and mounted in a 0.7-mm quartz capillary. Other crystals were soaked in an artificial mother liquor containing cacodylic acid (50 mM, pH 5.0) instead of citrate or in a solution containing 500 mM glucose 6-phosphate, adjusted to pH 5.0 with phosphoric acid. These crystals were also mounted in 0.7-mm quartz capillaries.

Data Collection. Crystals were irradiated with X-rays generated by an Eliot GX-6 rotating anode (30 kV × 30 mA) with a 0.5-mm focusing cup and 0.3-mm collimation. The crystals were kept at a temperature of 4 °C during the X-ray experiment by placing them in a stream of chilled air. Diffraction spot intensities were recorded on a Siemens X-100A multiwire proportional X-ray detector as the crystal was oscillated 0.2° per frame. The crystals were irradiated for an average of 5 min per frame, and the detector swing angle was set to collect data from 0° to 52° (∞ to 1.76 Å). Diffraction was initially detectable beyond 52°, but these reflections decayed rapidly and were deemed more appropriate to be collected at higher X-ray flux. Several orientations of the crystals were used to assure completeness; the statistics for reproducibility and data completeness are summarized in Table 1. At the selected swing angle, the crystal proved to be very robust in the X-ray beam, showing no more than 25% overall decay in intensity during data collection. The set of X-ray diffraction images was reduced to integrated indexed intensities and merged using the XDS and XSCALE programs, respectively (Kabsch, 1988).

Refinement of the Native Aldose Reductase Structure. Initial phases for the native structure were calculated from rigid body refinement of preliminary unrefined protein and cofactor coordinates provided to us by F. A. Quiocho. Using these phases, an initial electron density map ($3|F_o|-|2F_c|$) was calculated using the program XPLOR (Brünger, 1992) and displayed on an Evans and Sutherland PS340 using the program FRODO (Jones, 1978). While the α-helices and β-sheets were recognizable and the $NADP^+$ was distinct, many of the loops and surface side chains were clearly out of density. The initial *R*-factor of this model after rigid body refinement was 36% at 2.0-Å resolution. The model was manually rebuilt using FRODO. Regions of the map surrounding residues 20, 125, and 224 were at this stage not interpretable and were thus omitted from the model. The model was refined using all data to a nominal 2.0-Å resolution with the program XPLOR using a 3000K simulated annealing protocol. After group *B*-factors were refined, the *R*-factor dropped to 28%.

Difference Fourier maps with coefficients ($3|F_o| - |2F_c|$) and ($|F_o| - |F_c|$) were calculated and examined, and several side-chain placements were adjusted to fit the electron density. The electron density around residue 20 was interpreted and included in the new model, which was then refined using "positional" least-squares refinement. The new phases gave electron density maps which could be used to fit further the residues around residue 20, as well as the amino acids around residue 125. Other amino acids were also rebuilt so as to fit their electron density. Positional refinement continued to clarify the electron density, until the region around amino acid 125 could be well fit. The amino acids around position 20 then were omitted, and an "annealed omit map" was generated (Hodel et al., 1992), which allowed this region to be fitted for the final time. The region surrounding amino acid 224 still required much work; however, these amino acids were tentatively included in the model at this time.

After this round of complete manual rebuilding followed by positional refinement, the model including all of the amino acid side chains and individual *B*-factors gave an *R*-factor of 21.7% versus all data to 1.8-Å resolution. At this stage of refinement, we identified an area of electron density in the active site, previously noted but left unexplained (Wilson et al., 1992). The unexplained electron density was clearly too large to be a water molecule. To improve the phases of the electron density map, we fit water molecules to the residual electron density (except the unidentified electron density in the active site pocket) found in the difference Fourier (coefficients $|F_o| - |F_c|$) map. Electron density peaks greater than 3σ above the mean density of the map that had neighboring hydrogen bond donors or acceptors on the protein were automatically modeled as water molecules using the program WATERHUNTER (Sugio, personal communication).

Water molecules that were "found" in the unidentified electron density in the active site and those found near residue 224 were removed as they were judged to be unreliable. The *R*-factor dropped to 19.1%, and the unexplained electron density could be identified as a bound citrate molecule. An energy-minimized model of citric acid (both coordinates and molecular dynamics parameters) was generated by the program QUANTA (Molecular Simulations, Inc). The citric acid model was docked into the previously unexplained electron density, and after some of the torsion angles were adjusted, the citric acid fit the electron density well. Water molecules whose *B*-factor refined to greater than 35 $Å^2$ were discarded at this stage of the refinement. Positional refinement and manual rebuilding lowered the *R*-factor to 18%. Additional waters were generated using WATERHUNTER, but waters generated in the region of residue 224 were removed before any further refinement. An omit map of the region around residue 224 revealed a new tracing of that part of the backbone chain, which was then included in the model. Water molecules were manually added at this stage to fit residual 3σ peaks. Positional refinement followed by the refinement of individual *B*-factors produced our current model. Water molecules with *B*-factors greater than 40 $Å^2$ were excluded from the final round of refinement. The current model, including 160 bound water molecules, has been refined to an *R*-factor of 16.9% versus all observed data with intensities of $I/\sigma(I) > 1$ in the resolution range 10.0–1.76 Å.

Refinement of the Cacodylate-Soaked Aldose Reductase Structure. Refinement of the structure of the cacodylate-soaked enzyme crystal was simpler. Coordinates of the partially refined native structure were used to calculate initial phases. These were applied to the data from the cacodylate-soaked crystals and gave an *R*-factor of 28% prior to refinement. After rigid body refinement, the *R*-factor dropped to 23.4%, which allowed the identification of the cacodylate molecule, a 7σ electron density peak above background in the difference Fourier map ($|F_o| - |F_c|$), tetrahedrally surrounded by four 3σ protuberances. A model of cacodylate was generated and placed in the electron density. Automatic water location was used to place water molecules in the structure as described above. The model was refined using XPLOR's positional and individual *B*-factor refinement. The *R*-factor dropped to 19.2%, and manual rebuilding was begun. Residues in the vicinity of residue 224 again showed disorder; however, the rest of the structure fit the electron density well. An

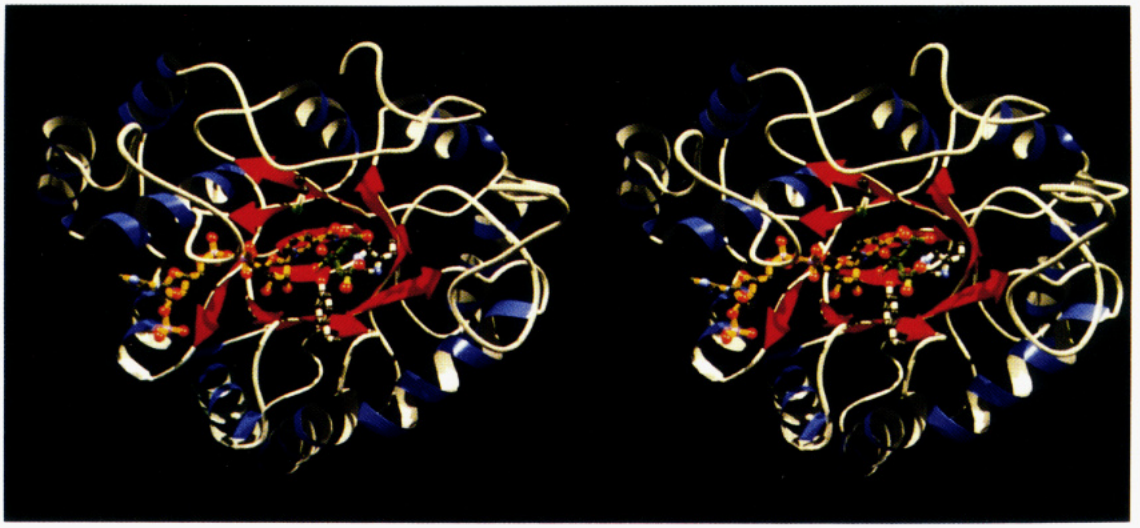

FIGURE 1: Stereo ribbon representation of the aldose reductase α-carbon chain. The overall fold is a TIM (triose isomerase), or α/β barrel [eight parallel β-strands (red) in sequential order connected by α-helices (blue)], with an $NADP^+$ cofactor (yellow) bound across the top of the C-terminus of the barrel. The nicotinamide ring along with the active site residues (Tyr48, His110, and Cys298 shown) is situated in the center of the barrel near the carboxy end of the β-strands. A pair of β-strands near the N-terminus of the protein form the bottom of the barrel. A large flexible loop (209–230) covers the diphosphate backbone of the cofactor.

annealed omit map of this region allowed refitting of this electron density. After positional refinement of the rebuilt model, water molecules were added by hand to "likely" 3σ peaks. The final aldose reductase–cacodylate complex model, including 150 bound water molecules, was refined to an R-factor of 17.6% versus all observed data with intensities of $I/\sigma(I) > 1$ in the resolution range 10.0–1.76 Å.

Refinement of the Glucose 6-Phosphate Soaked Aldose Reductase Structure. Initial phases for the glucose 6-phosphate soaked crystal were calculated from the partially refined native structure without the citrate in the active site. After rigid body and positional refinement of the structure, the R-factor was 22%. At this point, the position of the phosphate group of glucose 6-phosphate became clear, and a phosphate group was modeled to fit the electron density. Bound water molecules from the native structure were included in the refinement, and the R-factor dropped to 19%. Water molecules with B-factors greater than 40 $Å^2$ were removed from the model. After adjustments were made to the loop around residue 224 and further positional refinement, the remainder of the glucose 6-phosphate molecule was built into the electron density as a cyclic glucose. Additional waters were found and added to the water list by examination of the $(|F_o| - |F_c|)$ map and manual placement into electron density peaks that were over 3σ and that had hydrogen-bonding partners. The model of the aldose reductase–glucose 6-phosphate complex, including 181 bound water molecules, was refined to an R-factor of 16.6% versus all observed data with intensities of $I/\sigma(I) > 1$ in the resolution range 10.0–1.76 Å.

Enzyme Assays and Kinetic Analysis. Enzymatic activities were determined by measuring the rate of enzyme-dependent decrease of NADPH absorption at 340 nm in a Gilford Response spectrophotometer at 25 °C. The standard reaction mixture (1-mL volume) contained 0.2 mM NADPH, 1 mM DL-glyceraldehyde, or 100 mM xylose, in a 100 mM sodium phosphate buffer, pH 7.0. Kinetic constants were determined in the same way except the substrate concentrations were varied. The rate of the reverse reaction was determined by measuring the increase in the absorption at 340 nm. The reverse reaction mixture (1-mL volume) contained 0.2 mM $NADP^+$, xylitol, and 100 mM sodium phosphate buffer, pH 7.

Each data point (initial velocity) was determined in duplicate over at least six different substrate concentrations. Control assays, lacking either substrate or enzyme, were routinely included, and the rates were subtracted from the reaction rates. Kinetic constants were calculated by fitting the Michaelis–Menten function directly in hyperbolic form to the data with an unweighted least-squares analysis using the Marquardt–Levenberg algorithm provided with SigmaPlot, version 5.0. Steady-state kinetics in the presence of inhibitors were analyzed by the equation

$$v_i = VA/[K_m(1 + I/K_{is}) + A(1 + I/K_{ii})] \qquad (1)$$

where K_{is} is the slope (competitive) inhibitory constant, K_{ii} is the intercept (uncompetitive) inhibition constant, V is the maximal velocity, A is the substrate concentration, and K_m is the Michaelis–Menten constant. The inhibition pattern and a >5-fold relative difference between K_{is} and K_{ii} determined competitive or uncompetitive inhibition. Accordingly, either term in the equation was set to 1, and the fit for either K_{is} or K_{ii} improved significantly as judged from the standard errors and the sum of the residual least-squares values.

$NADP^+$/NADPH was stripped from the purified enzyme by incubation in 0.6 M $(NH_4)_2SO_4$ and gel filtration over a Bio-Gel P-10, 1 × 50 cm column (100–200 mesh, Bio-Rad Laboratories, Hercules, CA) primed with 3 mL of 0.6 M $(NH_4)_2SO_4$. The sample was chased with an additional 1 mL of the sulfate solution. A 5 mM NaP_i, pH 7.4, running buffer, containing 0.1 mM EDTA and 7 mM β-ME, was used, and the eluate fractions were collected and analyzed spectroscopically.

RESULTS

Structural Overview. Human aldose reductase belongs to the class of protein folds called the TIM barrel enzymes (Figure 1). The N-terminus of the protein (β-strands S1 and S2) forms a hairpin β-sheet that covers the bottom of the barrel. S3 begins the first of eight parallel β-strands that form the interior of the barrel. Helix H1 connects β-strands S3 to S4. The loop between S4 and H2 contains one of the active site residues, Tyr48. H2 leads to S5 which contains another active

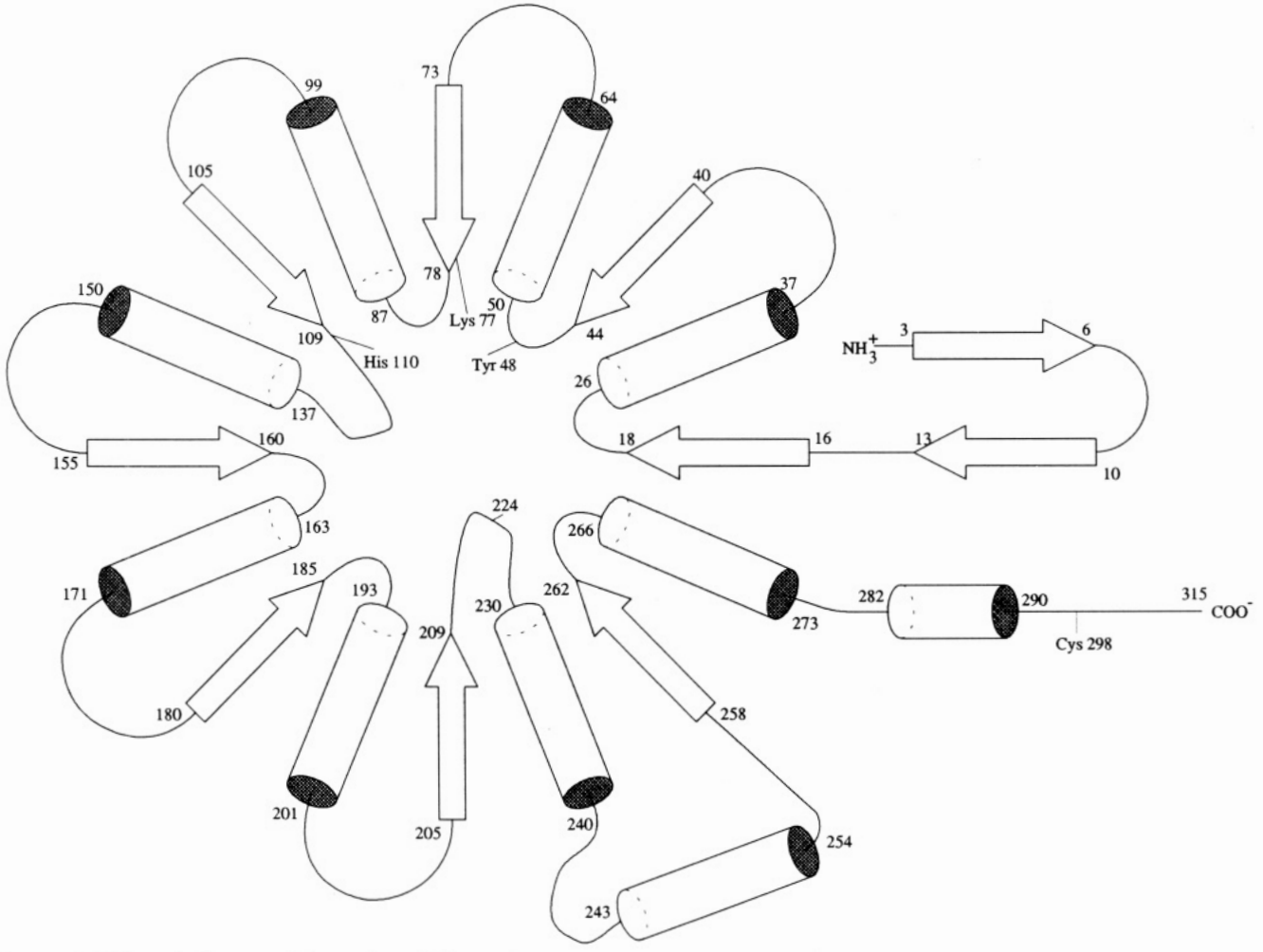

FIGURE 2: Schematic diagram of the topology of aldose reductase. Arrows represent β-strands and cylinders represent α-helices. The locations of active site residues are noted.

site residue, Lys77, which buries its charge in the body of the barrel. After a short loop, helix H3 begins and leads to S6. There is a large loop between S6 and H4 which contains both the active site residue His110 and the region around residue 125 (which was difficult to fit during refinement and has high *B*-factors). H4 leads to S7, H5, S8, and H6 which make no direct contributions to the active site. S9 provides active site residue Tyr209 and leads to a large loop region around residue 224, many of whose residues either make contact with or act to block bulk solvent from interacting with the nicotinamide cofactor. This loop has some of the highest *B*-factors in the molecule due to what we believe to be its flexible nature (Rondeau et al., 1992). A pair of helices (H7 and H8) lead to S10 which completes the β-barrel. Two additional helices (H9 and H10) wrap around S10 and H8 and lead to an elongated protein chain containing the active site residue Cys298 that leads to the C-terminus. This information is summarized in Figure 2.

The 314 α-carbon coordinates of human aldose reductase, provided by Dr. Quiocho (one residue was missing from the loop near residue 224) and used for initial phase determination, were compared with our final model. They showed an overall rms deviation of 2.35 Å. The maximum α-carbon$_{init}$ to α-carbon$_{final}$ deviation of 9.9 Å was observed at residue Lys221. However, when only the residues from the strands and helices of the barrel were compared, an overall rms deviation of 0.25 Å was observed. The individual hydrogen bonds and salt bridges to the nicotinamide cofactor shown earlier (Wilson et al., 1992) are in good agreement with this structure determination. However, we note in addition that the peptide nitrogen of Lys262 makes a hydrogen bond to one of the pyrophosphate oxygens of NADPH. The Nζ of Lys262 forms salt bridges to the oxygen (O1PR) of the C2′ phosphate of the ribose of the adenosine (2.8 Å) on one side and the OD1 of Asp216 (3.0 Å) on the other and is hydrogen bonded as well to two water molecules (designated 806 and 896). Clearly, both the Nζ of Lys262 and the phosphate of the ribose are exposed to the solvent, which may provide part of the mechanism of cofactor exchange.

Comparing all 315 α-carbons of the structure of aldose reductase soaked with glucose 6-phosphate to that of the citrate-bound wild-type crystal shows that the α-carbons have an overall rms deviation of 0.155 Å and a maximum deviation of 0.51 Å at Lys221. A comparison of the structure of the cacodylate-soaked enzyme to that of the wild type shows an overall rms deviation of the α-carbons of 0.095 Å with a maximum deviation of 0.66 Å at Lys221. Analyses of bond lengths and angles for all three structures show an average rms bond-length deviation of 0.013 Å and an average rms angle deviation of 1.91° (Table 1). From these analyses, we conclude that the average coordinate error in all three structures is ~0.2 Å.

There are three buried waters (designated 891, 808, and 782) in the structure of aldose reductase. Water 891 is within hydrogen-bonding distance (2.8 Å) from one of the carboxylic oxygens of Asp43. The other of the carboxylic oxygens forms a salt bridge (2.8 Å) with the Nζ nitrogen of Lys77. This water molecule, 891, is also within hydrogen-bonding distance

Table 1: Data Collection and Refinement Statistics

	native	cacodylate	glucose-6-PO_4
space group	$P2_12_12_1$	$P2_12_12_1$	$P2_12_12_1$
R_{merge} (%)	4.3	6.4	5.0
completeness (%)			
∞–6.0 Å	86.1	91.1	77.1
6.0–4.5 Å	89.6	93.3	89.2
4.5–3.0 Å	93.0	84.9	81.7
3.0–2.5 Å	93.8	83.7	74.4
2.5–2.0 Å	87.2	77.4	68.0
2.0–1.8 Å	48.6	39.7	56.8
reflections			
$I/\sigma(I) > 0$	61502	62455	63370
unique	23329	20882	20854
cell dimensions			
a (Å)	50.11	50.11	49.94
b (Å)	67.20	67.20	67.17
c (Å)	92.18	92.18	91.36
refinement resolution (Å)	10.0–1.76	10.0–1.76	10.0–1.76
R-factor (%)	16.9	17.6	16.6
rms deviation from ideal geometry			
bond lengths (Å)	0.016	0.012	0.012
angles (deg)	2.89	1.43	1.42

of the Nε of His41 (2.9 Å) and water 808 (2.8 Å). The relatively low B-factor of 8.7 Å^2 for water 891 is probably due to this hydrogen-bonding net. Water 808 forms a hydrogen bond (3.0 Å) with the Oε oxygen of Gln183 and another hydrogen bond with the Oγ oxygen of Thr207. Water 808 also has a relatively low B-factor of 8.4 Å^2. The third buried water is on the other side of the active site, 14 Å from water 808. There are four potential hydrogen bond donors or acceptors surrounding water 782. The backbone carbonyl oxygens of residues 78 and His111 are potential hydrogen bond acceptors located at a distance of 2.8 and 3.2 Å from water 782, respectively. The nitrogen Nε of His83 and the backbone amide nitrogen of Cys80 are potential hydrogen bond donors located at a distance of 2.9 and 3.2 Å from water 782, respectively. The B-factor of this water molecule is lower than many of the backbone atoms of the protein, presumably due to this tight hydrogen-bonding network.

Evidence That the Crystal-Bound Cofactor Is NADP$^+$. To determine the oxidation state of the nicotinamide moiety in the crystal, the absorbance at 340 nm of a solution containing NADPH under the crystallization conditions was measured. The half-life of NADPH was less than 24 h at pH 5.0, which is consistent with previously published work showing that the 5,6 double bond of the pyridine ring of NADPH is hydrated at low pH and loses its absorbance at 340 nm (Oppenheimer, 1982). However, there is no evidence of hydration of the nicotinamide ring in any of our crystal structures, suggesting that the cofactor is NADP$^+$, which, in contrast with NADPH, is quite stable in acid solution. Further evidence is provided by experiments whereby freshly prepared aldose reductase is extensively dialyzed against the 5 mM sodium phosphate buffer (pH 7.4) used in all chromatographic steps and then concentrated by ultrafiltration. The cofactor, stripped from the enzyme as described in Methods, is recovered quantitatively on a molar basis. The recovered cofactor absorbs at 340 nm, indicating that it is NADPH. In other experiments, where the enzyme is first stored for 2 weeks at crystallization conditions (pH 5), the recovered cofactor does not absorb at 340 nm but shows absorbance at 260 nm, indicating that it is NADP$^+$.

The Active Site. Looking down the β-barrel of aldose reductase, the nicotinamide ring is tilted about 30° off the axis of the barrel, with the C4N atom pointed up toward the solvent. The A face of the ring faces the center of the barrel, and the B face of the ring is stacked up against residue Tyr209 from strand S9 of the β-barrel. The hydroxyl of Tyr48 is 3.4 Å away from the C2N atom of the nicotinamide A face. The plane of the tyrosine is nearly perpendicular to the plane of the nicotinamide ring. The Tyr48 OH, His110 Nε, and Lys77 Nζ atoms are found in a plane that is nearly parallel to the nicotinamide ring. The Nζ of Lys77 is 3.1 Å from the Tyr48 OH. In this NADP$^+$ crystal form of the enzyme (see below), Lys77 is buried (bulk solvent inaccessible) in the middle of the β-barrel and forms a salt bridge (2.8 Å) to Asp43 which is also buried. The His110 Nε nitrogen is 3.3 Å from the O7N oxygen of the nicotinamide. The sulfur atom of Cys298 is 4.1 Å from the C5N carbon and 4.2 Å from the hydride-accepting C4N carbon of NADP$^+$. Residue Cys298 is located nearly in the plane of the nicotinamide ring; however, the –SH group is on the B face of the ring.

Identification of the Active Site Electron Density as Citrate. In this structure determination, we observe the same unidentified electron density described by Wilson et al. (1992) within the active site pocket. This previously unexplained electron density is above the A face of the nicotinamide ring and near the C4N carbon. The electron density has been fit with a citrate molecule (Figure 3A). The average B-factor of the heavy atoms of citrate is 42 Å^2 with a standard deviation of 2 Å^2. The uniformly high B-factors for all atoms in the citrate molecule may indicate that the binding site is not fully occupied. The citrate is modeled so that the C3 carboxyl group has one of its oxygens pointing toward the C4N of the nicotinamide, the OH oxygen of Tyr48, and the Nε nitrogen of His110 (the distances are found in Table 2). The C3 hydroxyl group of citrate is 4.4 Å from the SH sulfur of Cys298. The pair of terminal carboxyl groups of citrate are within hydrogen-binding distance of each other, with their planes perpendicular to each other, so that the overall shape of the citrate molecule is nearly circular.

Replacement of Citrate with Cacodylate and Glucose 6-Phosphate. Further evidence that the previously unexplained electron density found in the original crystal structure is citrate comes from crystals that have been soaked with mother liquor containing cacodylate but not citrate. The shape of the electron density in this region is now dramatically different (Figure 3B). The highest peak (7σ) in the difference electron density map fits the arsenic atom of cacodylate. Once again, the average B-factor for the heavy atoms is high, 42 Å^2, with a standard deviation of 4 Å^2. As modeled, the distance from the cacodylate O1 oxygen to the Nε of His110 and to the OH of Tyr48 is 3.1 and 3.3 Å, respectively. The distance from the cacodylate O2 oxygen to the Nε of Trp111 is 3.0 Å. The methyl group C1 is surrounded by two water molecules at a distance of 3.3 Å each and is also near the Cε1 carbon of Tyr48 (3.5 Å). Two water molecules are near the methyl group C2, at distances of 2.8 and 3.0 Å. The modeling of the non-arsenic atoms in cacodylate is somewhat arbitrary, since it is possible to interchange C2 and O2 given the distances involved.

The electron density within the active site pocket has a different shape again when the substrate molecule glucose 6-phosphate is substituted for citrate (Figure 3C). The phosphate binds very close to where the cacodylate binds, and its electron density is again unambiguous. The glucose part of the molecule extends toward the solvent and is probably represented in a number of configurations. The major cyclic configuration is modeled in Figure 3C. Considering the poor quality of the electron density, it is surprising that the overall

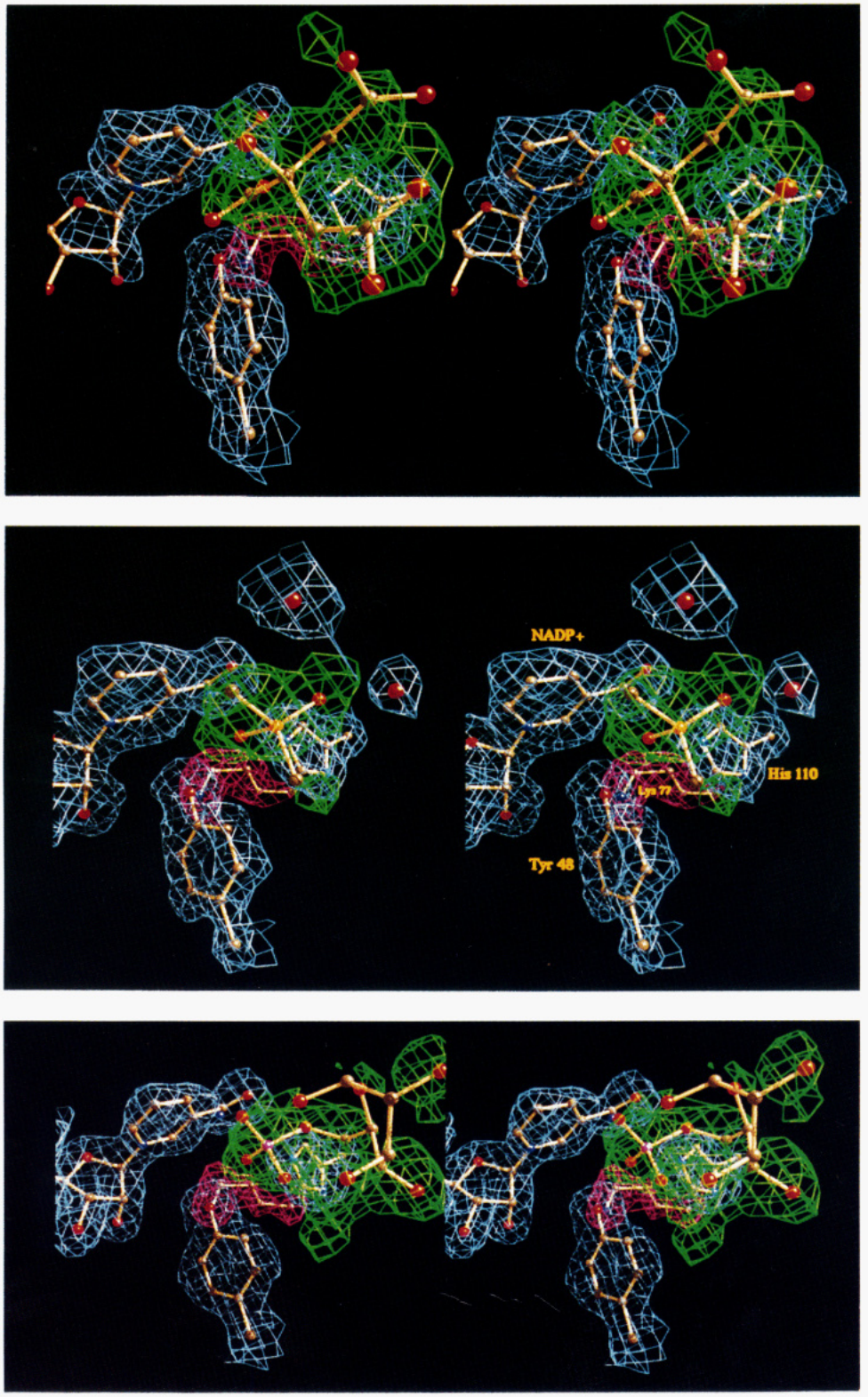

FIGURE 3: Stereo ball-and-stick model of the active site of aldose reductase with each of three small molecules bound within the active site (carbon = gray, nitrogen = blue, oxygen = red, phosphorus = magenta, and arsenic = yellow). Each model is enclosed in a wire-cage representation of the electron density, which is at least 0.8σ above the average electron density of the map as calculated by a Fourier transform using $2|F_o| - |F_c|$ as coefficients. The blue-colored electron density surrounds the active site residues and the $NADP^+$ cofactor. The magenta-colored electron density surrounds Lys77, which may be playing a role in polarizing the active site. The green-colored electron density surrounds the citrate (A, top), cacodylate (B, middle), and glucose 6-phosphate (C, bottom) molecules.

B-factor (38 ± 7 Å^2) is comparable to that of the other two compounds. However, unlike citrate and cacodylate, the *B*-factors are not uniform throughout the molecule. The *B*-factors of the phosphate group are much lower than those of the glucose moiety. The relatively high *B*-factors in the glucose moiety are probably due to the conformational freedom available to this group relative to the phosphate. It is also possible that the low phosphate *B*-factors are due in part to inorganic phosphate present in the artificial mother liquor that is competing for this binding site.

Table 2: Distances to Active Site Residues (Å)

	110 Nε	48 OH	C4N
citrate			
O16	2.78	3.37	3.19
O17	4.67	3.51	3.75
C6	3.87	3.86	3.63
cacodylate			
O	3.18	2.87	3.08
glucose 6-phosphate			
O	2.87	2.91	3.27

A Potential Anion Site. The superimposed positions of all three molecules bound in the active site pocket are shown in Figure 4. There appears to be a common binding site for the negative charge of each of these three molecules. The site is bounded by the hydroxyl group of Tyr48, the nitrogen Nε of His110, and the C4N of the nicotinamide ring. A list of distances from these residues to the attractant component(s) of each molecule is provided in Table 2. For citrate, there is a resonance sharing of the negative charge between the two oxygens of the C3 carboxylate; thus although the O16 oxygen of citrate is closer to the position of the negatively charged oxygens of the other compounds, both the O16 and O17 oxygen distances are noted.

Inhibition of Aldose Reductase by Citrate. Figure 5A shows the Lineweaver–Burk double-reciprocal plot indicating uncompetitive inhibition with respect to the aldehyde by citrate in the forward reaction (reduction of D-xylose) at pH 7.0 and $K_{ii} = 9.9 \pm 0.4$ mM. Figure 5B shows that the citrate inhibition in the reverse reaction (oxidation of xylitol), pH 7.0, is competitive with respect to the alcohol; $K_{is} = 4.5 \pm 0.3$ mM.

Citrate inhibition of aldose reductase in the forward reaction is pH-dependent as shown in Table 3, with the strongest inhibition occurring at the lowest pH tested, pH 5.0. The enzyme is activated by citrate at and above pH 8. Thus at pH 8, k_{cat} for the reduction of DL-glyceraldehyde by aldose reductase increases 30% in the presence of 50 mM citrate. Cacodylate does not inhibit the wild-type enzyme at either pH 5 or pH 7; in fact, the enzyme is activated up to 25% in the concentration range tested (up to 100 mM). Glucose 6-phosphate is a substrate for aldose reductase. The $K_{m(G6P)}$ at pH 7.0 is 230 ± 10 mM, with $k_{cat} = 0.2$ s^{-1} and $k_{cat}/K_m = 0.9$ M^{-1} s^{-1}. Comparable values for D-glucose are 80 ± 8 mM, 0.25 s^{-1}, and 3.1 M^{-1} s^{-1}, respectively. Glucose 1-phosphate is not a substrate but an uncompetitive inhibitor with respect to the aldehyde (D-xylose), with a K_{ii} of 141 ± 7 mM at pH 7. Inorganic phosphate activates the rate of catalysis linearly with k_{cat} increasing from 0.33 ± 0.01 to 0.45 ± 0.01 s^{-1} over the range of 30–120 mM at pH 7. The activation of aldose reductase by inorganic phosphate is slightly and progressively reduced at pH 8 and pH 9.

Effect of Citrate, Sulfate, and Phosphate Polyanions on Aldose Reductase and the K262M Mutant Enzyme. The activation of wild-type enzyme by citrate at pH 8 and by phosphate ions at pH 7 and pH 8 is reminiscent of the well-known activation of wild-type enzyme by sulfate ions (Hayman & Kinoshita, 1965). Although the mechanism of sulfate activation is not completely understood, it was shown to involve the Lys262 residue and enzyme–cofactor interaction. NADPH binding is markedly reduced in the K262M mutant enzyme with the apparent $K_{m(NADPH)}$ increased to 125 μM, and in contrast to the wild-type enzyme, it is inhibited by sulfate ions at pH 7 (Bohren et al., 1991). Table 3 shows that citrate inhibits the K262M mutant enzyme uncompetitively both at pH 6 (3.5 m) and at pH 8 (50 mM). Furthermore, in contrast to the wild-type enzyme, inorganic phosphate inhibits the K262M mutant enzyme at pH values of 6, 7, 8, and 9 (data not shown).

DISCUSSION

Aldose reductase reduces a diverse group of substances to their respective alcohols and is of special interest because of its involvement in the etiology of some diabetic and galactosemic complications. The catalytic mechanism of the human placental (Wermuth et al., 1982), the bovine kidney (Grimshaw et al., 1989), and the porcine skeletal muscle (Kubiseski et al., 1992) aldose reductases has been shown to be an ordered bi-bi reaction, in which NADPH binds to the apoenzyme, followed by subsequent binding of the aldehyde. The hydride of NADPH is transferred to the carbonyl carbon, and a proton is transferred to the carbonyl oxygen. The alcohol product is released, followed by the release of NADP$^+$. The exchange of cofactor is the major rate-determining step of the overall reaction (Grimshaw et al., 1990; Kubiseski et al., 1992).

Our recently determined structure of human aldose reductase (Wilson et al., 1992) showed that the cofactor is bound to the enzyme via a complex system of hydrogen bonds, salt bridges, and a large holding loop (residues 210–230) that virtually covers most of the cofactor with only portions of the nicotinamide and the phosphoribose exposed to the solvent. The structure of the porcine aldose reductase apoenzyme (Rondeau et al., 1992), crystallized in the absence of NADPH, shows that this loop is in an "open" configuration. These findings indicate that the enzyme undergoes a large conformational change involving this flexible loop. The correlation of the kinetically determined rate-limiting cofactor exchange with the structural data implies that this conformational change is a major component of the rate-limiting step.

Comparison to Dehydrogenase Mechanism. The reduction of an aldehyde to an alcohol using NADPH as a reducing agent may be compared to the back-reaction of an alcohol dehydrogenase. We have reviewed the mechanisms of many dehydrogenases and find that they fall into two classes, those which use Zn^{2+} as an electrophile and the 4-*pro-R* hydrogen of nicotinamide and those which use histidine to facilitate proton donation to the carbonyl oxygen (Walsh, 1979). There is no known metal ion requirement for aldose reductase nor is there any metal ion found in the crystal structure, ruling out the Zn^{2+} mechanism.

Cys298 is a possible choice as a nucleophile to catalyze the reduction of the aldehyde, but this possibility is ruled out by the location of the SH group and studies of the C298A and C298S mutants (Bohren & Gabbay, 1993; Petrash et al., 1993). The sulfhydryl group of Cys298 of aldose reductase lies on the B side of the plane of the nicotinamide ring and is 4.2 Å away from the C4N group and, thus, not optimally positioned to be directly involved in catalysis. Studies of the serine or alanine mutants of Cys298 (Bohren & Gabbay, 1993; Petrash et al., 1993) further confirm this conclusion.

Since the enzyme does not have an active site metal, and there is no evidence to support a sulfhydryl intermediate, an alternative mechanism is suggested by our results. All three compounds studied, citrate, cacodylate, and glucose 6-phosphate, have a common anion binding site in the crystal structure of the NADP$^+$ form of the enzyme. The presence of this anion binding site suggests a catalytic mechanism for the reduction of an aldehyde to a primary alcohol. There are two extreme reaction sequence possibilities for such a reduction: The first is a nucleophilic attack on an aldehyde carbonyl by a hydride followed by subsequent protonation of the negatively

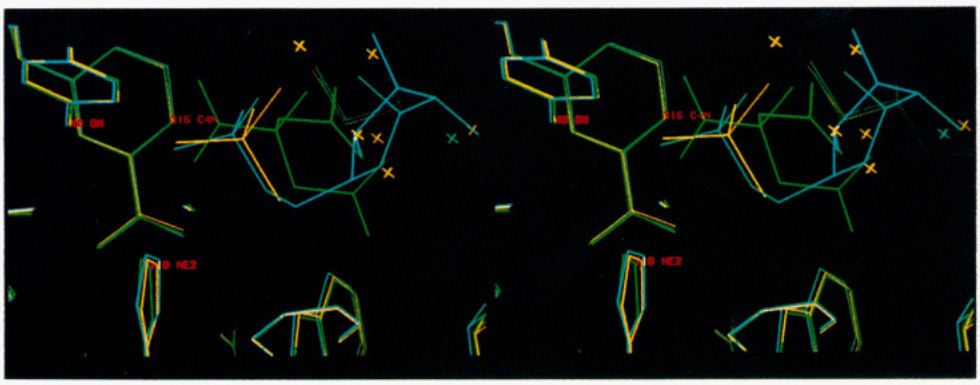

FIGURE 4: Stereo superimposition of the three aldose reductase active site pockets, with citrate, cacodylate, and glucose 6-phosphate, as seen from above the A face of the nicotinamide ring of the cofactor. The molecules were aligned by a least-squares fit of α-carbons 1–315. The citrate structure is shown in green, the cacodylate structure is displayed in yellow, and the glucose 6-phosphate structure is displayed in blue. Note that a negatively charged oxygen from each of these small molecules is found in the middle of a triangular plane formed by the C4N of the nicotinamide, the Nϵ of His110, and the OH of Tyr48.

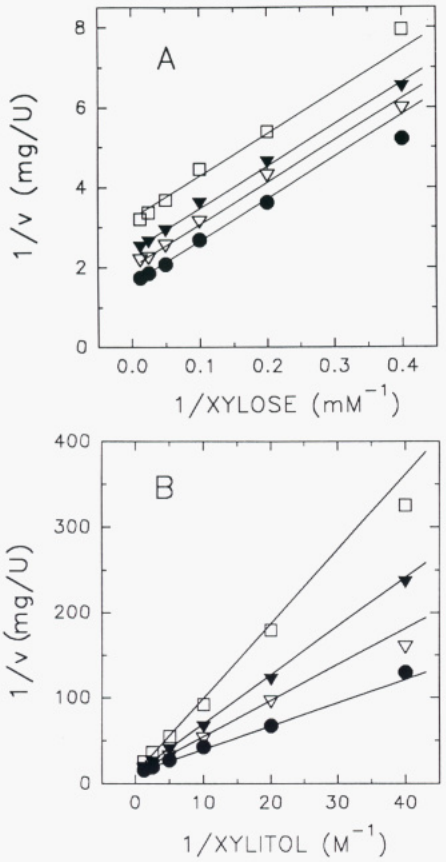

FIGURE 5: Inhibition of human aldose reductase by citrate. Double-reciprocal plots of the initial velocities are shown. Citrate concentrations are as follows: filled circles (0 mM), open triangles (2.5 mM), filled triangles (5 mM), and open squares (10 mM). Lines follow the fitted equation for uncompetitive inhibition in the reduction reaction of D-xylose (A) and for competitive inhibition in the oxidation reaction of xylitol (B).

charged oxygen of the resulting alkoxide ion (Figure 6). At the other extreme, the carbonyl oxygen is protonated followed by hydride transfer to the resulting carbonium ion. The common anion binding site in the structure of the NADP$^+$ form of the enzyme suggests that the active site may have evolved to stabilize a negatively charged species, such as the alkoxyl intermediate of the first mechanism. Alternatively, the carbonyl bond may be polarized by the local positive charge, thus promoting hydride attack in a concerted reaction. Neither steady-state kinetics nor protein crystallography can distinguish between these two mechanisms.

Table 3: Apparent Citrate Inhibition Constants for Wild-Type and K262M Aldose Reductases

	K_{ii} (mM)	
pH	wild type	K262M
5.0	0.17 ± 0.09	
6.0	0.86 ± 0.06	3.25 ± 0.25
7.0	9.40 ± 0.60	
8.0	activation	50 ± 7

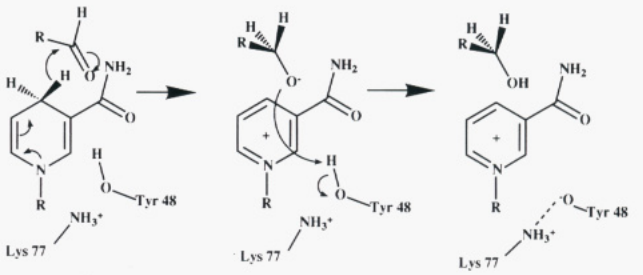

FIGURE 6: Possible aldehyde reduction mechanism involving a hydride nucleophilic attack on the carbonyl carbon of the aldehyde, followed by protonation of the resultant alkoxide. Note that the proton neutralizing the alkoxide is derived from the protein (Tyr48) and not the solvent.

The mechanism proposed is similar to that found in lactate dehydrogenase (LDH). LDH uses a histidine residue to either abstract a proton in the "forward" reaction or donate a proton in the "reverse" reaction. The histidine along with an arginine polarizes the carbonyl bond to facilitate hydride attack. An alignment of the nicotinamide ring of LDH with that of aldose reductase shows that His195 of LDH is located at the corresponding site where all three anionic molecules bind in aldose reductase. Inspection of the active site residues shows that the charge distribution in LDH is opposite in direction to that of aldose reductase. LDH has a large number of positive residues (some to bind the carboxylate of lactate) on the C4N side of the nicotinamide ring, whereas aldose reductase has positively charged residues on the N1N side of the nicotinamide ring. Additionally, LDH binds the carboxylate group of pyruvate in a manner to direct the carbonyl oxygen away from the nicotinamide ring and toward the histidine. The structures of the aldose reductase–inhibitor complexes suggest that the carbonyl of the aldehyde should be directed toward the nicotinamide ring, perhaps being positioned directly above the ring itself before the hydride attack. While it is possible that His110 in aldose reductase plays the same role as His195 of LDH, this is unlikely given that the LDH mechanism

requires that the histidine has conformational freedom to exchange protons with the solvent, and His110 of aldose reductase does not have that freedom. Furthermore, the presence of three adjacent hydrophobic residues (Val47, Trp79, and Trp111), and the proximity to Lys77 (4.8 Å), may impart a low pK_a to His110, making the formation of the imidazolium ion unlikely at physiological pH and rendering its role in proton donation improbable. Mutagenesis studies reported in the accompanying paper indicate that Tyr48 is the proton donor in aldose reductase (Bohren et al., 1994).

Inhibition and Activation of Aldose Reductase. The binding of citrate in the active site suggested that it may be a novel aldose reductase inhibitor. Indeed, studies show that citrate at pH 5 is an uncompetitive inhibitor of the enzyme with respect to the aldehyde in the forward direction and a competitive inhibitor with respect to the alcohol in the reverse direction (Figure 5). If the citrate molecule with two negative charges (pK_{a2} = 4.8, pK_{a3} = 6.4) is binding in the alcohol (product) binding site, it would be expected that the inhibition of the reverse reaction will be competitive and of the forward reaction, uncompetitive. The kinetic studies of citrate inhibition described above indicate that it is competing directly with the alcohol product in the enzyme–NADP$^+$ active site, and thus its position in our refined crystal structure can be used to define that site.

At pH 8.0, citrate is an activator of aldose reductase (Table 3), like other polyanions such as sulfate and phosphate, while at acidic pH, it is an inhibitor. Our data suggest the existence of multiple anion binding sites in aldose reductase similar to the anion well existing at the alcohol binding site of the NADP$^+$ form of the enzyme. Another anion binding site appears to be present in the vicinity of two groups that are exposed to the solvent, the Nζ of Lys262 and the C2′ phosphate of the adenosine ribose of NADP, which interact via hydrogen bonding. We earlier showed that mutation of the positively charged K262 to methionine affects NADPH binding and increases $K_{m(NADPH)}$ 66-fold and k_{cat} 2-fold. In contrast with activation of the wild-type enzyme, the K262M mutant enzyme is in fact inhibited by sulfate at pH 7 (Bohren et al., 1991). As with sulfate, both citrate and phosphate inhibit the K262M mutant enzyme at pH 8 as well as at acidic pH, suggesting a similar interaction of the two polyanions with Lys262. We propose that these polyanions (and inorganic phosphate as well) share a common activation mechanism, namely, competitive binding to Lys262 with respect to the C2′ phosphate of the adenosine ribose of the cofactor. Such competitive interaction would be expected to weaken the binding of the coenzyme and result in a more rapid exchange rate and, hence, the observed increase in turnover (2-fold increase in k_{cat}).

Identification of the negatively charged citrate molecule within the crystal structure led us to look for and find other anions that bind to the active site of aldose reductase. Cacodylate also binds to the active site of the enzyme. Interestingly, it does not show inhibition of the wild-type enzyme but is instead a weak activator between pH 5 and pH 8, activating the enzyme with a maximum of 25% at pH 5 (data not shown). Glucose 6-phosphate also binds to the active site of the enzyme and is, in fact, a substrate for the enzyme, although it is not as good a substrate as glucose itself. It is possible that the "backward", unproductive, conformation that we observe in the crystal structure (NADP$^+$ form of the enzyme) with the phosphate bound in the active site pocket is one reason that it is a poor substrate. It is interesting to note that glucose 1-phosphate, which is not a substrate, is in fact an uncompetitive inhibitor with respect to the aldehyde in the forward reaction. We speculate that its phosphate group binds to the enzyme in a manner analogous to that of glucose 6-phosphate.

Stereochemistry of the Reaction. While it is established that the hydride is coming from the A face of NADPH in aldose reductase (Feldman et al., 1977) during catalysis, the proton comes from either the solvent or one of two possible donor residues in the protein's active site. It has been shown that the *re* face of glyceraldehyde receives the hydride, which also occurs in the case of horse liver alcohol dehydrogenase (Walsh, 1979). Vander Jagt et al. (1992), using placental human aldose reductase, showed that acetol is reduced to L-1,2-propanediol while methylglyoxal is reduced to either acetol (95%) or D-lactaldehyde (5%). The reduction product of the ketone group in both of these cases does not show a detectable amount of the other enantiomers, i.e., D-1,2-propanediol or L-lactaldehyde, which indicates that the nature of the group at the β-carbon of the substrate determines which face of the carbonyl is attacked.

Both methylglyoxal and acetol can be modeled in the active site of the enzyme by aligning the ketone carbonyl with that of the corresponding oxygen–carbon bond in citrate while keeping the plane of the molecule parallel to the plane of the nicotinamide ring. The substrate may have its *re* face or its *si* face toward the nicotinamide. When acetol is correctly positioned for hydride attack, the hydroxyl group corresponding to the aldehyde group of methylglyoxal is positioned to interact with the Nϵ of His110. When methylglyoxal is positioned so that the resulting hydride attack would give D-lactaldehyde, the aldehyde carbonyl group does not interact with His110. Thus, the ability of the hydroxyl group of acetol to donate a hydrogen bond to the Nϵ of His110 directs the stereochemistry of the reaction.

From the modeling studies, it appears that His110 directs the stereochemistry of the hydride attack. Using this model, it is difficult to explain how the Nϵ nitrogen of His110 can act both as a hydrogen bond acceptor for directing the stereochemistry of the product and as a proton donor to the oxygen of the emerging alcohol. Therefore, Tyr48 is suggested to be the proton donor. Although the pK_a of tyrosine is normally very high (pK_a 10.5), this may be modified by the environment of the residue in the protein. In the case of Tyr48, the Nζ of the buried Lys77 is 2.8 Å from the OH of tyrosine, and its positive charge could lower the pK_a of the tyrosine, making it a better proton donor.

The serendipitous use of citrate in the crystallization buffer plus its identification within the enzyme active site and as an inhibitor of the enzyme has led us to propose a working hypothesis for the catalytic mechanism of aldose reductase. The mechanism proposes that an aldehyde substrate binds with its carbonyl group located in an active site pocket formed by His110, Tyr48, and the C4N of the nicotinamide ring. This anion binding site polarizes the carbonyl bond for subsequent hydride attack and proton transfer from the putative proton donor, Tyr48. Product release and cofactor exchange complete the cycle.

NOTE ADDED IN PROOF

Wilson et al. (1993) reported the structure of an inhibitor, zopolrestat, bound to the aldose reductase holoenzyme. Because of an embargo of the coordinates for this structure, a direct comparison with our data has not yet been carried out. Nevertheless, the published pictures show that the negatively charged carboxylate of zopolrestat is bound to the anion well, apparently similarly to the carboxylate of citrate

and the negatively charged cacodylate and glucose 6-phosphate, thus confirming the singular and central nature of the anion well.

ACKNOWLEDGMENT

We are grateful to Dr. Charles E. Grimshaw for helpful discussions and to Daniel Peisach for his development and help in the use of the computer programs that generated Figures 1 and 3. We thank Ragini Shankar and Stephen Henry for their technical assistance.

REFERENCES

Bachur, N. R. (1976) *Science 193*, 595–597.
Bohren, K. M., & Gabbay, K. H. (1993) *Adv. Exp. Med. Biol. 328*, 267–277.
Bohren, K. M., Bullock, B., Wermuth, B., & Gabbay, K. H. (1989) *J. Biol. Chem. 264*, 9547–9551.
Bohren, K. M., Page, J. L., Shankar, R., Henry, S. P., & Gabbay, K. H. (1991) *J. Biol. Chem. 266*, 24031–24037.
Bohren, K. M., Grimshaw, C. E., & Gabbay, K. H. (1992) *J. Biol. Chem. 267*, 20965–20970.
Bohren, K. M., Grimshaw, C. E., Lai, C.-J., Harrison, D., Ringe, D., Petsko, G. A., & Gabbay, K. H. (1994) *Biochemistry* (following paper in this issue).
Brünger, A. T. (1992) XPLOR Software, Yale University, New Haven, CT.
Brünger, A. T., Kuriyan, J., & Karplus, M. (1987) *Nature 235*, 458–460.
Feldman, H. B., Szczepanik, P., Havre, P., Corrall, R. J. M., Yu, L. C., Rodman, H. M., Rosner, B. A., Klein, P. D., & Landau, B. R. (1977) *Biochim. Biophys. Acta 480*, 18.
Gabbay, K. H. (1973) *N. Engl. J. Med. 288*, 831–836.
Grimshaw, C. E., Shahbaz, M., Jahangiri, G., Putney, C. G., McKercher, S. R., & Mathur, E. J. (1989) *Biochemistry 28*, 5343–5353.
Grimshaw, C. E., Shahbaz, M., & Putney, C. G. (1990) *Biochemistry 29*, 9947–9955.
Hayman, S., & Kinoshita, J. H. (1965) *J. Biol. Chem. 240*, 877–882.
Hodel, A., Kim, S.-H., & Brünger, A. T. (1992) *Acta Crystallogr. A48*, 851–859.
Jones, T. A. (1978) *J. Appl. Crystallogr. 11*, 268–272.
Kabsch, W. (1988) *J. Appl. Crystallogr. 21*, 916–924.
Kador, P. F. (1988) *Med. Res. Rev. 8*, 325–352.
Kinoshita, J. H. (1974) *Invest. Ophthalmol. 13*, 713–724.
Kubiseski, T. J., Hyndman, D. J., Morjana, N. A., & Flynn, T. G. (1992) *J. Biol. Chem. 267*, 6510–6517.
Oppenheimer, N. J. (1982) in *The Pyridine Nucleotides* (Everse, J., Anderson, B., & You, K., Eds.) pp 51–86, Academic Press Inc., New York.
Petrash, J. M., Harter, T., Tarle, I., & Borhani, D. (1993) *Adv. Exp. Med. Biol. 328*, 289–300.
Rondeau, J.-M., Tete-Fâvier, F., Podjarny, A., Reyman, J.-M., Barth, P., Biellmann, J.-F., & Moras, D. (1992) *Nature 355*, 469–472.
Vander Jagt, D. L., Robinson, B., Taylor, K. K., & Hunsaker, L. A. (1992) *J. Biol. Chem. 267*, 4364–4369.
Walsh, C. (1979) *Enzymatic Reaction Mechanisms*, Chapter 10, W. H. Freeman & Co., San Francisco, CA.
Wermuth, B., Bürgisser, H. P., Bohren, K. M., & von Wartburg, J.-P. (1982) *Eur. J. Biochem. 127*, 279–284.
Wilson, D. K., Bohren, K. M., Gabbay, K. H., & Quiocho, F. A. (1992) *Science 257*, 81–84.
Wilson et al. (1993) *Proc. Natl. Acad. Sci. U.S.A. 90*, 9847–9851.